CHAPTER 2

Experimental Section :

2.0 Introduction :

This chapter describes the experimental setup and also explains the working principles of different experimental techniques used in our studies in details.

2.1 Electrochemical cell :

A conventional three-electrodes electrochemical cell was used in our study. The cell is made of glass with a teflon lid machined to fit with the B-55 size neck. This lid can accommodate the working, reference and counter electrode. There is also provision of gas inlet and outlet for deaerating the cell. For the experiment in ethanol, an electrochemical cell with a provision for Saturated Calomel Electrode (SCE) in a separate compartment connected by Luggin capillary was used. The cell was cleaned thoroughly before each experiment and kept in a hot air oven at 100 ^{o}C for at least 1 hour before the start of the experiment. Before each experiment, the electrolyte in the cell was completely deaerated by passing oxygen-free nitrogen gas. During the experiment, a blanket of nitrogen gas was maintained on top of the solution.

2.2 Electrodes :

In our study, we have used gold electrode as working electrode. A platinum foil of large surface area was used as counter electrode. A Saturated Calomel Electrode (SCE) was used as reference electrode in aqueous media, whereas a silver rod was used as a quasi-reference electrode in different non-aqueous

solvents like acetonitrile [1,2], propylene carbonate, formamide etc. SCE was also used as reference electrode in ethanol kept in a separate compartment connected by Luggin capillary. The silver quasi-reference electrode has a potential of –0.2 V with respect to SCE [3] in acetonitrile. This electrode has a stable potential in non-aqueous solvents and is also free of any liquid junction potential.

2.3 Preparation of working electrode & electrode pre-treatment :

In most of the electrochemical studies, we have used gold disk macro and microelectrodes. We have fabricated all the electrodes used in our studies. The gold disk electrode was fabricated by proper sealing of a 99.99 % pure gold wire (Arora Mathey) of 0.5 mm diameter with soda lime glass having thermal expansion coefficient close to that of gold. We have also fabricated disk shaped gold and platinum microelectrodes with diameters of 10-50 μm by sealing sodalime glass with metal microwires. The gold and platinum microwires (diameters 10, 12.5, 40 and 50 μm) were obtained from Advent (U.K). The detailed method of fabrication of these microelectrodes and the composition of the sodalime glass will be described in the later chapter (Chapter 6). All these electrodes show no leakage when kept in electrolytes even for days, which indicates excellent metal-glass sealing. Immediately before use, the gold electrode was polished using aqueous slurries of progressively finer alumina (1.0, 0.3, 0.05 μm sizes), sonicated to remove the alumina particles and rinsed in distilled water. Finally, the electrode was chemically etched using dilute aqua regia (3:1:4 ration of concentrated HCl, concentrated HNO_3 and water). This procedure had been shown to yield a substrate with the best blocking properties for supporting self-assembled

monolayer of alkanethiols [4,5]. Before monolayer formation, the electrode was thoroughly washed with millipore water.

2.4 Preparation of evaporated Au substrate :

Evaporated gold substrates on glass were used for electrochemical impedance spectroscopic and Grazing Incidence FT-IR spectroscopic studies. Evaporation of gold (~100 nm thickness) on glass was carried out using vacuum evaporation unit (Hindhivac) at a pressure of 2×10^{-5} mbar. Chromium underlayers (2-5 nm thickness) were deposited on glass before gold evaporation to improve the adhesion of gold on glass. The substrate was heated to 350^{0} C during gold evaporation, a process which normally yields a substrate with predominantly Au (111) orientation. The gold samples were used as strips for electrochemical studies with a well defined area exposed to the electrolyte solution, rest of the portion being insulated with parafilm and teflon. These gold samples were cleaned with Piranha solution (mixture of concentrated sulphuric acid and 30% hydrogen peroxide in 3:1 ratio) for 30s before each experiment and finally rinsed in millipore water.

2.5 Preparation of Au substrate obtained by replica technique :

For STM studies, the substrates were prepared using a novel replica technique from the evaporated gold on mica [6,7]. We find from literature that the replica technique has been employed by Diebel et al. [8] to obtain ultra-smooth gold and silver surfaces on different substrates like mica, float glass, polymer coated silicon etc. These surfaces had a root mean square roughness down to 0.2 nm over micrometer areas as observed from their STM experiment [8]. These surfaces can be used as substrates for the

monolayer formation of thiol molecules. In our case, these ultra-smooth gold surfaces were obtained by electroplating about 200 μm thick copper on the evaporated face of the gold surface on mica and finally peeling off the plated layer from mica to get a much smoother surface. We have performed STM experiment [6,7] on these gold substrates. These surfaces are very much smooth and crystalline with average domain height of 2-4 nm. Figure 1 shows the 100 nm × 100 nm constant current STM image of gold substrate on mica obtained by replica technique.

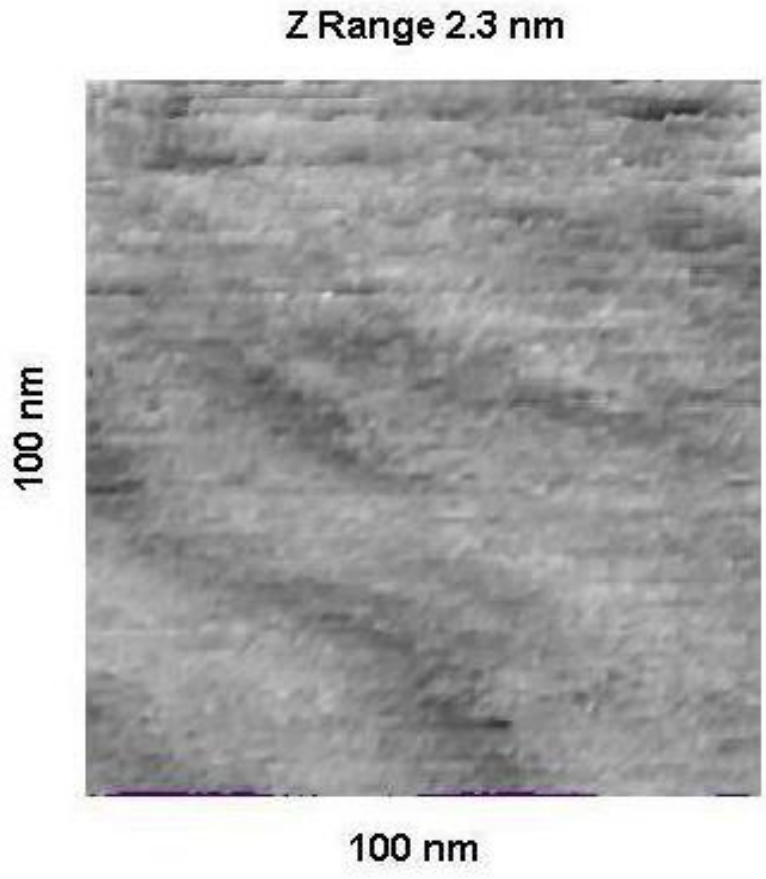

Fig. 1 : Constant current STM image of bare gold surface prepared by replica technique : Tunneling current : 0.5 nA, Bias voltage: Sample + 100 mV, Scan range : 100 nm × 100 nm

2.6 Experimental techniques :

In our studies, we have used electrochemical techniques like cyclic voltammetry and electrochemical impedance spectroscopy and non-electrochemical techniques like grazing angle FT-IR spectroscopy and Scanning Tunneling Microscopy (STM).

2.6.1 Cyclic voltammetry :

Among the potential sweep techniques, cyclic voltammetry is the most common and widely used technique to study the reaction mechanism of redox reaction. This popular electroanalytical technique deals with the scanning of the potential of working electrode between potential limits V_1 & V_2 at a scan rate ν with forward and reversed scan and measuring both the faradaic current due to oxidation or reduction reaction (faradaic reaction) of electroactive species in the solution and the capacitive current due to double layer charging [9,10]. The plot of current as a function of potential range is known as cyclic voltammogram.

Kinetic parameters and mechanisms of different heterogeneous reactions and coupled homogeneous reactions and different surface processes like adsorption, desorption, passivation and deposition can be studied using cyclic voltammetry technique. The shape of cyclic voltammogram depends on the type of redox reaction. For a typical reversible redox reaction of the type $O + ne^- \rightleftharpoons R$, the rate of charge transfer is always greater than rate of mass transfer at all potentials and therefore Nernstian equilibrium is always maintained at the electrode surface. Near the electrode surface in the Nernst diffusion layer region, the concentration gradients of electroactive species is linear. The ratio of surface concentration of O and R is given by Nernst equation. So as the potential becomes more

negative, the surface concentration of O decreases progressively. Therefore, the concentration gradient and the current also increases. Eventually, the surface concentration of O becomes zero. At that moment, the concentration gradient and current become maximum. However, the concentration gradient starts to decrease due to diffusion and current also decreases. Overall, this behaviour gives rise to a peak shaped voltammogram. Using similar arguments, it can be shown that the reversed sweep also gives rise to a peak. The peak current I_p of cyclic voltammogram is given by Randles-Sevcik equation.

$$I_p = -0.4463nF\left(\frac{nF}{RT}\right)^{1/2} c_o^{\infty} D^{1/2} \nu^{1/2}$$

where,

I_p is the peak current density in $A\,cm^{-2}$,

D is the diffusion coefficient in $cm^2\,\sec^{-1}$

ν is the sweep rate in $V\,\sec^{-1}$

n is the number of electrons involved in the reaction

F is Faraday constant

R is gas constant

T is the absolute temperature.

At 25^0 C the above equation reduces to the form,

$$I_p = -\left(2.69\times 10^5\right) n^{3/2} c_o^{\infty} D^{1/2} \nu^{1/2}$$

From the above equation, it can be seen that for a reversible reaction the peak current is proportional to the concentration of electroactive species and also the square root of scan rate. A test of the reversibility of the system is to check whether a plot of I_p as a function of $\nu^{1/2}$ is both linear and passes

through the origin.[or alternatively $(I_p/\nu^{1/2})$ is constant]. For a reversible system:

a) $\Delta E_p = \left|E_p^A - E_p^C\right| = \frac{59}{n}\ mV$

b) $\left|E_p - E_{p/2}\right| = \frac{59}{n}\ mV$

c) $\left|\frac{I_p^A}{I_p^C}\right| = 1$

d) $I_p \propto \nu^{1/2}$

e) E_p is independent of ν.

f) At potentials beyond E_p, $I^{-2} \propto t$.

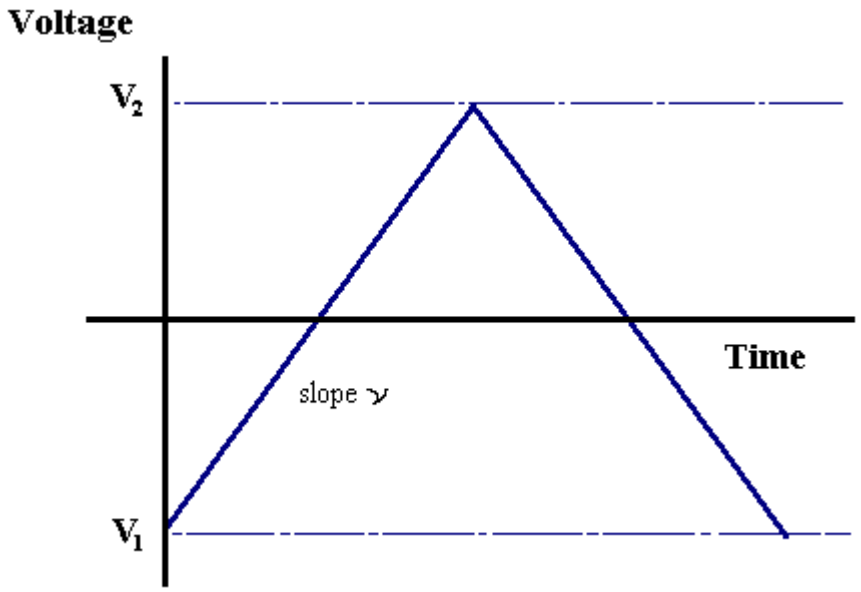

Potential – time profile for cyclic voltammetry

We have used the cyclic voltammetry technique extensively in our studies using conventional size macroelectrodes and microelectrodes. Microelectrodes have several advantages for cyclic voltammetry. Due to the small electrode area of microelectrode, the current associated with microelectrode is very small, of the order of nA to pA and the current

densities are very high [11]. Due to this small current, the ohmic drop (iR drop) and the double layer charging current is extremely small and the cyclic voltammogram is unaffected by these two factors. Hence, microelectrodes are used to carry out cyclic voltammetry at extremely high scan rates (10^6 Vs^{-1}) [12] and even in high resistive media [13].

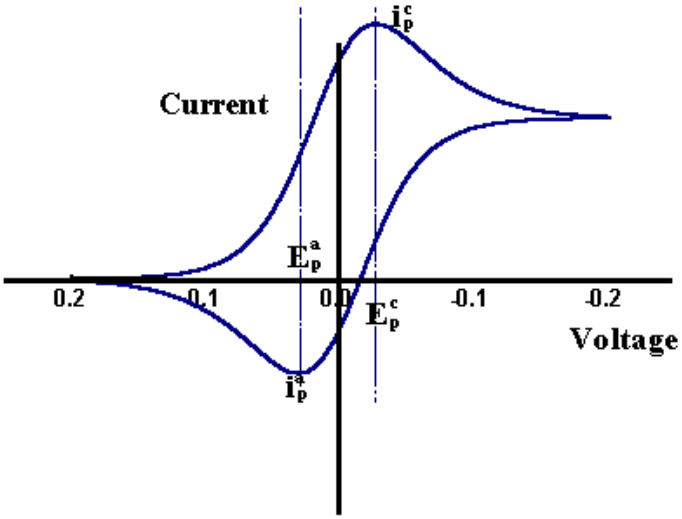

Cyclic voltammogram for a reversible process

Cyclic voltammetry can be employed to determine the real surface area of metal electrode by measuring the charge of oxide stripping or hydrogen adsorption peak.

The real surface areas of electrodes of transition metals like Pt, Rh, Ir are determined from the measurement of the charge of voltammetric peak of hydrogen adsorption or desorption in a potential regions prior to hydrogen gas evolution [14,15]. The charge associated with the adsorption of one hydrogen atom on each metal atom on the surface is Q_H. On the other hand, the charge associated with a one to one H-M correspondence per unit surface area Q_H^s is calculated on the basis of distribution of metal atoms at the surface. For polycrystalline Pt, the accepted value of Q_H^s is 210 $\mu C\ cm^{-2}$ on

the basis of the assumption that the density of atoms on the surface is 1.31×10^{15} cm^{-2}. So the real surface area = $\frac{Q_H}{Q_H^S}$. This method can not be used with metals adsorbing hydrogen such as Pd. This method is also not applicable to highly oxidizable transition metals like Ni, Os, Ru, Fe due to problem of overlapping of hydrogen and oxygen adsorption regions.

The method of real surface area measurement based on oxygen adsorption [14] is applicable to metals like gold which exhibits oxide monolayer formation and stripping peaks. Oxygen is assumed to be chemisorbed in a monoatomic layer prior to oxygen evolution with a one-to-one correspondence with surface metal atoms. Hence, the charge associated with the formation or stripping of the oxide monolayer is :

$$Q_0 = 2\,e\,N_A\,\Gamma_0\,A$$

where ,

N_A is Avogadro's number

Γ_0 is the surface concentration of atomic oxygen ,assumed to be equal to N_M , the surface density of metal atoms.

From the value of N_M per unit area the value of $Q_0{}^s$, the reference charge can be calculated. For polycrystalline gold, this value is 400 μC cm^{-2}. So the real surface area = $Q_0 / Q_0{}^s$. Hence, the roughness factor = real area / geometric area. We have calculated the roughness factor of working electrodes as measured by potential cycling in 0.1 M perchloric acid.

2.6.2 Electrochemical Impedance Spectroscopy :

This method involves small perturbation of electrode potential from equilibrium by the application of small sinusoidal signal to the

electrochemical cell and measurement of the response, that is the current which differs in phase and amplitude from the applied signal. Measurement of the phase difference and amplitude (impedance) over wide frequency allows analysis of different electrode processes related to diffusion, kinetics, double layer charging etc. This technique is widely used in the study of corrosion, battery, solid electrolytes, membranes etc.

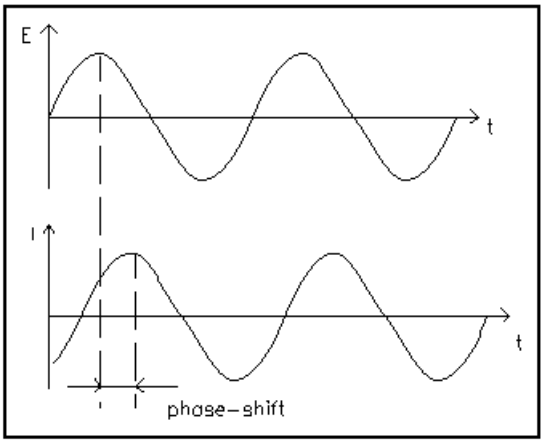

Sinusoidal current response in a linear System

Due to the small perturbation the electrochemical system is considered to be linear and linear current-potential characteristics are observed.

Before understanding the response of an electrochemical system to an ac perturbation, the basic principles of AC circuit is essential. If a sinusoidal voltage $V=V_o \sin \omega t$ is applied to an electrical circuit composed of resistors and capacitors, the current response is given by $I=I_o \sin (\omega t+\phi)$, where ω is the frequency, ϕ is the phase angle between the perturbation and response. The impedance Z is the proportionality factor between V and I. In case of a pure resistor R, ϕ is zero and there is no phase difference between V and I. For a pure capacitor, $I= C\, dV/dt$ or $I = V_o C\omega \sin(\omega t+\pi/2)$,

or $I=V_o /X_c \sin(\omega t+\pi/2)$. X_c is called capacitive reactance. So current leads the potential by $\pi/2$. The impedance $Z(\omega)$ of the electrochemical interface is

a complex number which can be expressed in either polar coordinates or in Cartesian coordinates. $Z = |Z| e^{j\phi}$ and $|Z|^2 = (\mathrm{Re}\, Z)^2 + (\mathrm{Im}\, Z)^2$ where $\mathrm{Re}\, Z$ and $\mathrm{Im}\, Z$ are the real part and the imaginary part of the impedance.

$$\phi = Arc\tan\frac{\mathrm{Im}\, Z}{\mathrm{Re}\, Z}$$

$$\mathrm{Re}\,(Z) = |Z|\cos\phi$$

$$\mathrm{Im}\,(Z) = |Z|\sin\phi$$

The electrode-electrolyte interface of the electrochemical cell can be represented by a suitable equivalent circuit consist of resistors and capacitors. A typical equivalent circuit is shown in the following figure.

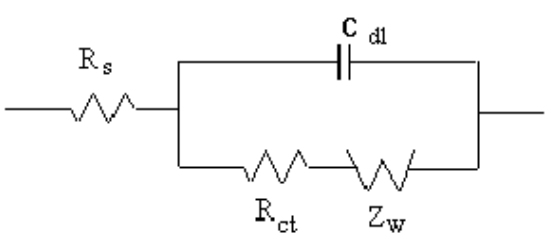

Randles equivalent circuit for an electrode reaction with double layer capacitance C_{dl}, charge transfer resistance R_{ct} , Warburg impedance Z_W and solution resistance R_s

The total current is considered to be the sum of faradaic current i_f and double layer charging current i_c. The double layer capacitance C_{dl} exists between the electrode-electrolyte interface. The faradaic impedance can be separated into the charge transfer resistance R_{ct} and the Warburg impedance Z_W which represents a kind of resistance to mass transfer because of diffusion. This impedance depends on the frequency of the potential perturbation. At high frequencies, the Warburg impedance is small, since diffusing reactants do not have to move very far. At low frequencies, the reactants have to diffuse very far, thereby increasing the Warburg impedance. R_s is the uncompensated solution resistance between the

working electrode and reference electrode. Since all the current must pass through the uncompensated resistance, R_s is inserted as a series element to represent this effect in the equivalent circuit. In contrast to R_s and C_{dl} which are nearly ideal circuit elements, the components of faradaic impedance are not ideal because they change with frequency ω. The full analysis of equivalent circuit and determination of individual components of it originated from the procedure long used in electrical engineering and it was first adapted to electrochemical applications by Sluyters et al [16]. This is the so-called ***Complex plane impedance analysis***. A full analysis of this series-parallel configuration, usually called the ***Randles equivalent circuit*** [17] has two limiting cases. At low frequencies as $\omega \rightarrow 0$ the real and imaginary parts of impedance are found to be:

$$Z' = R_s + R_{ct} + \sigma \omega^{-1/2}$$

$$Z'' = \sigma \omega^{-1/2} + 2\sigma^2 C_{dl}$$

where, $\sigma = \frac{RT}{\sqrt{2} n^2 F^2 A D^{1/2}} \left(\frac{1}{c_0^\infty} + \frac{1}{c_R^\infty} \right)$ D is the diffusion coefficient for the species in the solution

A area of the electrode

c_0^∞ and c_R^∞ are the bulk concentrations of the oxidised and reduced species, from which, $Z'' = Z' - R_s - R_{ct} + 2\sigma^2 C_{dl}$

This is the equation of a straight line of unit slope and with an intercept on the real Z' axis of , $R_s + R_{ct} - 2\sigma^2 C_{dl}$. At high frequencies, where the Warburg impedance is negligible in relation to R_{ct} the two components are:

$$Z' = R_s + \frac{R_{ct}}{1 + \omega^2 C_{dl}^2 R_{ct}^2}$$

$$Z'' = \frac{C_{dl} R_{ct}^2 \omega}{1 + \omega^2 R_{ct}^2 C_{dl}^2}$$

Eliminating ω gives

$$\left(Z' - R_s - R_{ct}/2\right)^2 + \left(Z''\right)^2 = \left(R_{ct}/2\right)^2$$

which is the equation of a circle centered on $Z' = R_s + R_{ct}/2$ with a radius of $R_{ct}/2$.

A plot of the whole expression for Z'' versus Z' for kinetic controlled reaction has the following form (Cole-Cole plot).

Cole-Cole plot

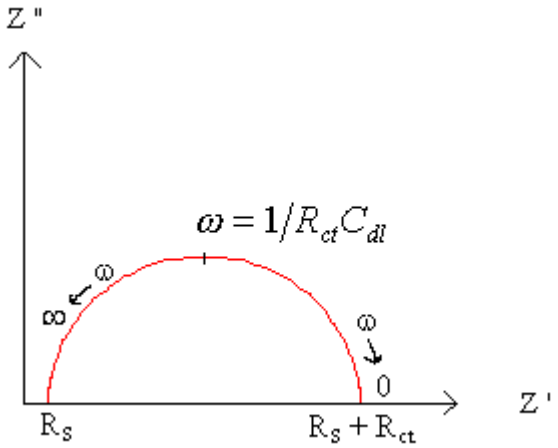

At infinite frequency, Z''approaches zero as the capacitance in the equivalent circuit offers very little impedance. At low frequencies the impedance is purely resistive, because the reactance of C is very large. The solution resistance has the effect of translating the semi circle on the Z'axis. R_s can be found by reading the real axis value at the high frequency intercept. C_{dl} is obtainable from the maximum value of Z'' in the semi circular region where $\omega = 1/R_{ct}C_{dl}$ .The diameter of the semi circle is given by R_{ct}. Another way of presenting impedance data is by the Bode plot [18].

In this, logarithm of the modulus of impedance $\log|Z|$ and the phase angle ϕ are both plotted in the y-axis with a common abscissa of log of frequency. On such a plot, a pure resistance is represented by a horizontal line and a constant ϕ of 0^0, while a pure capacitor is a straight line of slope –1 and a constant ϕ of -90^0.The Bode plot for Randles equivalent circuit (without Warburg impedance) is shown in the following figure.

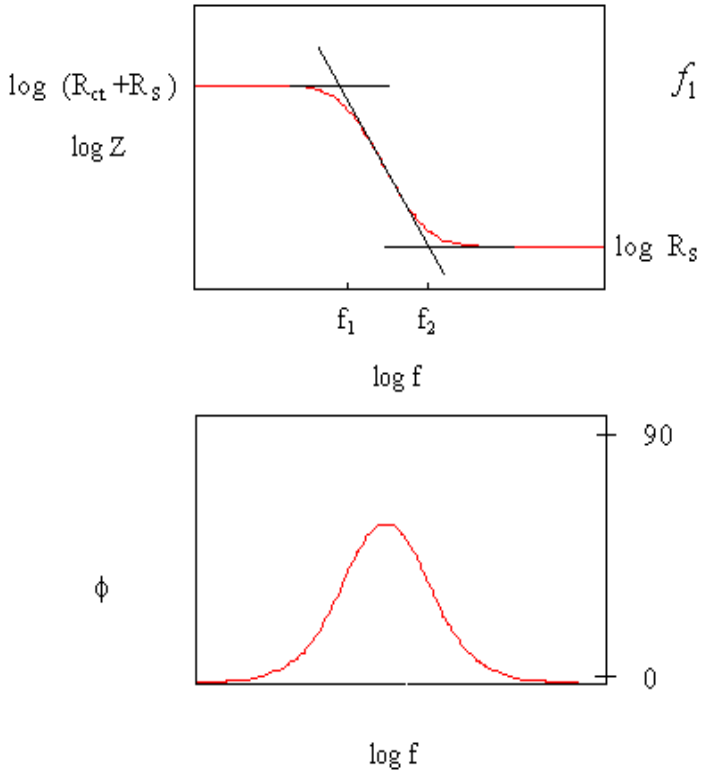

$$f_1 = \frac{1}{2\pi(R_{ct} + R_S)C}$$

$$f_2 = \frac{1}{2\pi R_S C}$$

Bode plot

When electrochemical systems possess more than one time constants, then it is better to present the impedance in Bode plot rather than the Cole-cole plot.

There are different types of methods used to measure impedance. We have used the method of phase sensitive detection by lock–in amplifier to measure the impedance of the electrochemical cell. The potential of the working electrode is held at the desired potential of interest using a potentiostat. A small amplitude sinusoidal voltage input is applied to the cell

from a lock-in amplifier. The current output from the cell has a phase difference with respect to the input voltage. The lock-in amplifier measures this phase difference and amplitude of the current response.

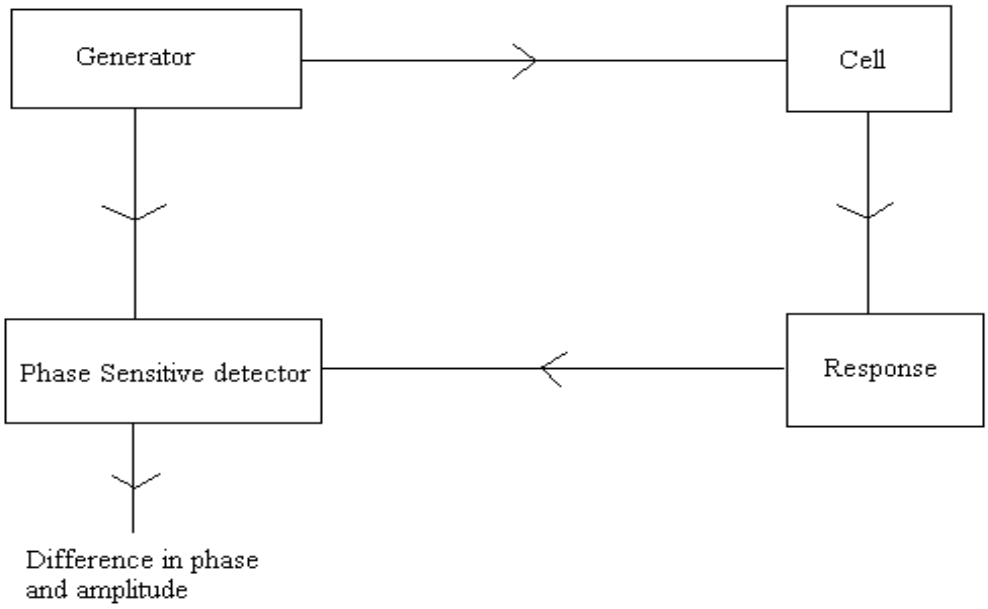

Schematic diagram of Phase Sensitive Detector

The elements of an equivalent circuit model represent the various macroscopic processes involved in the transport of mass and charge in electrochemical system. The dispersion relations for most of the circuit elements are very simple. If the dispersion diagrams show distinct features that can be easily related to specific physical processes and can be defined to different sub-circuits of the equivalent circuit, the analysis becomes quite simple. However, if the time constants associated with different sub-circuits are relatively close together on the time axis, or if elements with fractional (<1) power dependence on frequency (e.q. Warburg or a Constant Phase Element) are present, then the dispersion curve becomes convoluted. A more sophisticated analysis method is required as the variation of one circuit parameter can affect large parts of frequency dispersion, and hence affects

the parameters of other sub-circuits. All parameters in the equivalent circuit model are adjusted simultaneously by using Non Linear Least Squares Fit techniques (NLLSF). Using these techniques, one can obtain the optimum fit to the measured dispersion data. A thorough treatment of these procedure was done by Bevington [19].

In our studies, the impedance data were analyzed using the Boukamp's impedance software [20] by fitting to an appropriate equivalent circuit. This software has been written by Bernard A. Boukamp in Turbo Pascal (version 3.0) programming language. Impedance data were also analyzed using the ZsimpWin EIS DATA analysis software (Perkin Elmer, version 2.00).

2.6.3 Grazing Angle FT-Infrared Spectroscopy :

FT-IR spectrometers record the interaction of IR radiation with a sample, measuring the frequencies at which the sample absorbs the radiation and the intensities of the absorptions. Determining these frequencies allows identification of the sample's chemical structure and nature of functional groups, as chemical functional groups absorb radiation at particular frequencies. The intensity of the absorption are represented in a two-dimensional plot called IR spectrum. Intensity is generally reported in terms of absorbance, the amount of light absorbed by a sample, or percentage of transmittance, the amount of light that passes through the sample. Frequency is expressed in terms of wave numbers. The key components of a FT system are the source, the interferometer and the detector. The interferometer provides a means for the spectrometer to measure all optical frequencies simultaneously, modulating the intensity of individual frequencies of radiation before the detector picks up the signal. The product of an interferometer 'scan' is called an interferogram, a plot of intensity versus

mirror position. Using the mathematical process of Fourier Transform, a computer converts the interferogram into a spectrum.

In addition to bulk samples, FT-IR can be used in surface studies mainly to study molecular packing and ultrathin organic films [21,22]. The spectrum is obtained using either internal or external reflection modes. The internal reflection mode is known as the (ATR) Attenuated Total Reflection Spectroscopy, whereas the external reflection mode is known as Reflection-absorption or Grazing Angle Spectroscopy. Attenuated Total Reflection (ATR) is a multiple internal reflectance technique and is explained in details by Griffiths et al [23]. The beam is directed onto an angled crystal and reflected within it until it emerges from the other end where it is collected. The number of reflections is dependent upon the angle of incidence upon the crystal. The crystal is usually made of KRS-5, Zinc Selenide, or Germanium. Grazing Angle Reflection or External Reflection technique provides a nondestructive method for measuring surface coatings. External reflectance is a mirror like reflection from the surface of a sample. The infrared radiation is directed onto the surface of a sample at an angle of incidence I. For external reflectance angle of reflection, R, is equal to angle of incidence, I. The amount of radiation reflected depends on the angle of incidence, refractive index of the sample, surface roughness of the sample and the absorption properties of the sample. The angle of incidence is selected depending on the thickness of the coating which is being studied. For very thin coatings in the nanometer thickness range like ultrathin organic films, an angle of incidence 85-88^0 is used. Reflectance measurements at this angle of incidence are often referred as grazing angle measurements. For samples with coatings of micrometer thickness range, a 30^0 angle of incidence is normally chosen. The reflection-absorption spectrum for a monolayer

adsorbed on a metal surface is measured mostly at higher angle of incidence, and only allows the p-polarization component of incident light to pass [24]. The p-polarization component is parallel to the plane of incidence. The s-polarization component of incident light is perpendicular to the plane of incidence. Hence, the s-polarization component of incident light does not interact with ultrathin film samples on metal and therefore does not contribute to the spectral signal. This results in very high quality, clean spectra. The spectrum obtained on an ultrathin organic film coated metal substrate is ratioed with a suitable blank spectrum (taken on a bare substrate) to obtain the absorbance spectrum of the monolayer. The relative intensities of the absorption peaks in the spectrum are affected by the average orientation of transition dipoles relative to surface. A transition dipole parallel to the metal surface will exhibit a greatly attenuated peak relative to the transition dipole perpendicular to the metal surface. From these comparisons, the average orientation of the monolayer chains and the terminal groups are obtained. Peak positions also give information about the dynamic behaviour of the monolayer.

In our studies, the IR spectra were obtained using FT-IR 8400 model (SHIMADZU) with a fixed 85^0 grazing angle attachment (FT-85: Thermo Spectra-Tech). The FT-85 grazing angle attachment does not use mirrors like conventional specular reflectance accessories. Instead, it uses silicon refracting optical elements with the existing beam divergence in the sample compartment to obtain a high, 85^0 angle of incidence. The unique design of the FT-85 also features built-in polarizing elements. The silicon refracting elements are positioned at angles which allow only p-polarization to pass. Samples are placed on the horizontal sampling surface of the accessory. Therefore, no clamps are necessary. The sample area is approximately 10

mm wide and 40-50 mm long. The FT-85 is available for most popular FT-IR spectrometers and is easily installed with minimal alignment. The accessory is baseplate mounted to ensure reproducible sampling.

2.6.4 Scanning Tunneling Microscopy :

Scanning Tunneling Microscopy (STM) is a versatile tool in the area of surface science. It was invented by Gerd Binnig and Heinrich Rohrer [25] at the IBM research institute in Zurich. STM has the advantage of studying atomically smooth conducting surfaces in a variety of environments like Ultra High Vacuum (UHV), air, electrolytic media etc. The basic principle of STM is based on the tunneling of electrons across the insulating gap (either air or vacuum) between a chemically inert, sharp metallic tip like Pt-Ir/Rh, Pt, W and a conducting material usually a metal or a semiconductor by the application of a small bias voltage, when the tip is brought very close (~1 nm) to the sample without any physical contact. As a result, a small current (pA to nA) flows between the tip and the conducting sample [26]. Actually, the STM image corresponds to a contour map of local density of states of atoms on a conducting sample. The tunneling current is very much sensitive to the distance between the tip and sample. There is a change of current of an order of magnitude for a change of gap separation by 0.1 nm. The tunneling current is of the form $I_t \approx Ve^{-Cd}$ where I_t is the tunneling current, V is the bias voltage, C is a constant that includes the work function of the material and d is the spacing between the lowest atom on the tip and the highest atom on the sample. The strong exponential dependence of the tunneling current on the tip-to-sample spacing makes it possible to use this current in a feedback loop controlling a precision motion device; i.e. a piezoelectric scanner. In response to an applied voltage, the scanner moves

the tip over an area of the sample in a raster pattern and the feedback loop causes the tip to track the sample surface with sub-angstrom precision. The coordinates of the tip's path can then be transformed into a map of the surface topography. The STM can be operated either in constant current or in constant height mode. In the constant current mode of operation, the tip height above the sample is adjusted in such a way by the application of a feedback voltage that the current will remain constant, and the image is obtained as a map of this feedback voltage versus the lateral x & y coordinates. In the constant height mode, the tip is scanned over a sample in the same plane without adjusting the tip height. As a result, the tunneling current will change as a change of tip-sample separation. So the current is recorded as a function of lateral coordinates. This technique is generally used on atomically smooth conducting surfaces only. In our work, we have carried out STM studies using a home built instrument [27].

In designing and fabricating the STM, various important factors like efficient vibration isolation, minimum thermal drift, proper feedback control, atomically sharp STM tips preparation and coarse positioning of the tip are taken into account [27].

Since the tunneling current is in the order of nA to pA, measurement of such a small current and obtaining good resolution STM image requires vibration free environment. This can be achieved by increasing the resonance frequency of the STM scan unit such as using tube piezo scanners, which can eliminate both external or internal low frequency vibrations. The rigidity of the scan unit is one of the important factors in the vibration isolation system. It is mounted inside a nylon block with a hole and is secured by two screws to a cylindrical PVC block. The whole assembly is screwed onto a thick brass plate and is mounted onto a stack of three more

brass plates each separated by a viton O-ring. The entire assembly is suspended using a bungee chords to the ceiling to damp low frequency vibrations.

The thermal drift of the STM is compensated by proper selection of materials and symmetric design of scan unit.

Sharp tips are prepared by electrochemical etching of inert metal wires such as W or Pt-Rh or Pt-Ir. The Pt-Rh wire of 0.25 mm diameter is ac etched in an electrolytic solution of 5% each of NaCl and $NaNO_3$, whereas W tips are prepared by etching in 5% KOH solution. The tip obtained by this method is dipped in HF solution to remove any surface oxide, rinsed in distilled water and dried before inserting the tip into tip holder.

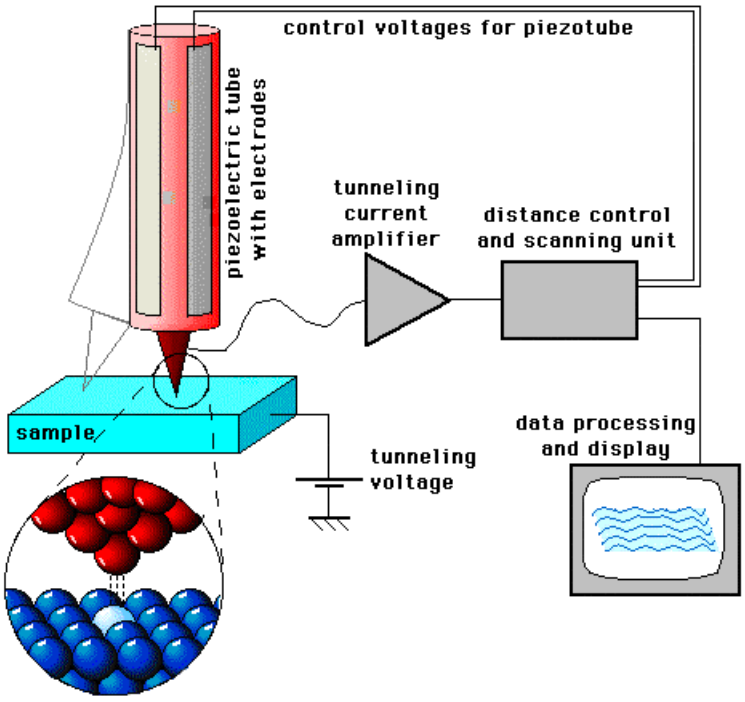

Schematic diagram of STM

The coarse positioning is achieved by inertial sliding mechanism, based on horizontal motion of the sample stage. The scan unit is built of two concentric piezo electric tubes, the inner one for scanning the tip and the outer one for moving the sample holder towards or away from the tip. The

piezo tubes are coated with silver both on outside and inside. The inner piezo tube holds the tip coaxially. The coarse positioning is achieved by applying a saw tooth waveform to the outer piezo tube. This will compress the tube and as a result the glass tube containing the sample holder is brought closer to the tip. During the slow rise of wave form, the sample stage essentially follows the piezo motion, while during the falling portion of the wave form the glass tube attached to the piezo quickly retracts. But the sample holder can not retracts due to inertial forces. As a result, the sample holder is translated towards the tip by one step. By applying a train of saw tooth pulses of amplitude 120 V and fast scan rate, speeds of about 1 mm/s both towards and away from the tip are achieved.

The STM can be operated either in constant current or in constant height mode. In the constant current mode of operation, the tip height above the sample is adjusted in such a way by the application of a feedback voltage that the current will remain constant, and the image is obtained as a map of this feedback voltage versus the lateral x & y coordinates. For constant current mode, the feedback control unit plays very important role. The feedback control unit compares the actual tunneling current with the user specified reference current. When the measured current is very large, the feedback conrol unit generates a voltage which is applied to the piezo tube scanner to pull the tip back from the sample and vice versa. The piezo tube expands linearly with the applied voltage, which is directly proportional to the changes in the vertical tip position.

STM electronics mainly consists of the current amplifier, analog feedback system, data acquisition using A/D and the piezo drivers comprising of the D/A card interfaced to a PC and high voltage amplifiers. The current amplifier is a high impedance operational amplifier AD 529,

which converts current into voltage over a 10 MΩ metal film resistance. This provides an output voltage of 10 mV for a current of 1 nA. The bias voltage is applied to the sample from the battery through the non-inverting input of the current amplifier. The output of the current amplifier is further amplified by 10 times using an instrumentation amplifier AD 624. An absolute value circuit (AVC) comprising two low noise OPA 27 op-amps provides the positive voltage to the logarithmic amplifier (AD 759 N). The logarithmic amplifier is used to linearize the exponential behaviour of the current response. A set of five high voltage operational amplifiers (APEX PA42) drive the piezo tubes for coarse positioning and X-Y scanning. This amplifier has maximum voltage operation of 350 V and output current of 120 mA.

A personal computer interfaced with a Keithly 500A measurement and control system consist of a 16 channel, 16 bit A/D card and two 2 channel, 16 bit D/A cards are used for data acquisition and control. Two of the D/A outputs are used for coarse positioning and Z control, while the other two are used for X-Y scanning. The STM line scan image is displayed in real time. All the images shown in this thesis are raw data images except for plane correction using Scanning probe image processor software (Image Metrology , Denmark). Before each experiment the STM is calibrated using atomic resolution images of ZYA grade HOPG (Advanced Ceramic Co, USA). Fiqure 2 shows the 2 nm × 2 nm constant current image of Highly Oriented Pyrolytic Graphite (HOPG). The hexagonal symmetry pattern of graphite lattice is clearly seen.

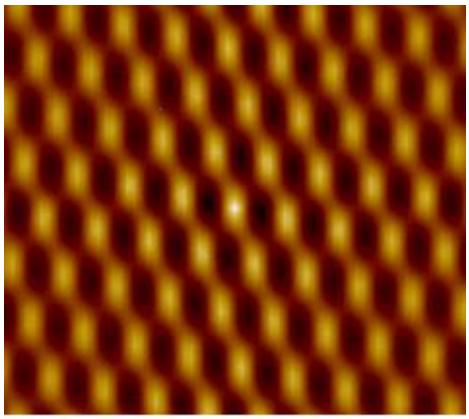

Fig. 2 Constant current STM image of HOPG: Tunneling current : 1 nA, Bias voltage : Sample + 100 mV, Scan range : 2 nm × 2 nm

REFERENCES

1. A. Fitch, D.H.Evans, *J.Electroanal.Chem.*, 202 (1986) 83
2. D.O.Wipf, R.M.Wightman, *Anal.Chem.*, 60 (1988) 2460
3. R.A.Malmsten, C.P.Smith, H.S.White, *J.Electroanal.Chem.*, 215 (1986) 223
4. S.E.Creager, L.A.Hockett, G.K.Rowe, *Langmuir*, 8 (1992) 854
5. E.Boubour, R.B.Lennox, *J.Phys.Chem.B*, 104 (2000) 9004
6. U.K.Sur, V.Lakshminarayanan, *Proc.of seventh International Symposium on Advances in Electrochemical Science and Technology*, SAEST, CECRI, INDIA, 27-29 November, Chennai, 2002, p B24-B27
7. U.K.Sur, V.Lakshminarayanan, *J.Colloid Interface Sci.*, 254 (2002) 410
8. J.Diebel, H.Lowe, P.Samori, J.P.Rabe, *Appl.Phys.A*, 73 (2001) 273
9. A.J.Bard, L.R.Faulkner, *Electrochemical Methods- fundamentals and applications*, Wiley, New York, 1980
10. *Instrumental methods in Electrochemistry*, Southampton Electrochemistry Group, Ellis Horwood Limited, 1990
11. *Microelectrodes : Theory and Applications*, M.I.Montenegro, M.A.Queiros, J.L.Daschbach (Eds.), NATO ASI series, Vol. 197, Kluwer, Dordrecht, 1991
12. J.O.Howell, R.M.Wightman, *J.Phys.Chem.*, 88 (1984) 3915
13. A.M.Bond, M.Fleischmann, J.Robinson, *J.Electroanal.Chem.*, 172 (1984) 11
14. S. Trasatti, O.A.Petrii, *Pure & Appl.Chem.*, 63 (1991) 711
15. *Comprehensive Treatise of Electrochemistry*, E.Yeager, J.O.M.Bockris, B.E.Conway, S.Sarangapani (Eds.), Vol.9, Plenum Press, 1981

16.J.E.B.Randles, *Disc. Faraday Soc.*, 1 (1947) 11

17.M.Sluyters-Rehbach, J.H.Sluyters, *Electroanalytical Chemistry*, A.J.Bard (Eds.), Vol.4, Ch.1, Marcel Dekker, New York, 1970

18.B.D.Cahan, C.T.Chen, *J.Electrochem.Soc.*, 129 (1982) 700

19.P.R.Bevington, *Data Reduction and Error Analysis for the Physical sciences*, McGraw-Hill, New York, 1969

20.B.A.Boukamp, *Equivalent Circuit Software*, Perkin Elmer, 2nd Edition

21.M.D.Porter, T.B.Bright, D.L.Allara, C.E.D.Chidsey, *J.Am.Chem.Soc.*, 109 (1987) 3559

22.C.E.D.Chidsey, D.N.Loiacono, *Langmuir*, 6 (1990) 682

23.P.R.Griffiths, J.de Haseth, *Fourier transform infrared spectroscopy*, Wiley Interscience, New York, 1986

24.J.F.Blanke, S.E.Vincent, J.Overend, *Spectrochim.Acta. Part A*, 32 (1976) 163

25.G.Binnig, H.Rohrer, Ch.Gerber, E.Weibel, *Appl.Phys.Lett.*, 40 (1982) 178

26.C.J.Chen, *Introduction to scanning tunneling Microscopy*, Oxford university Press, New York, 1993

27.V.Lakshminarayanan, *Curr.Sci.*, 74 (1998) 413